Bioorganic Chemistry 107 (2021) 104605

Contents lists available at ScienceDirect

Bioorganic Chemistry

journal homepage: www.elsevier.com/locate/bioorg

A colorimetric nano-biosensor for simultaneous detection of prevalent cancers using unamplified cell-free ribonucleic acid biomarkers

Hamidreza Mollasalehi [a,*], Elmira Shajari [b]

[a] Department of Microbiology and Microbial Biotechnology, Faculty of Life Sciences and Biotechnology, Shahid Beheshti University, Velenjak, Tehran Postal Code: 1983969411, Iran
[b] Protein Research Center (PRC), Shahid Beheshti University, Velenjak, Tehran, Iran

ARTICLE INFO

Keywords:
Cancer diagnosis
miRNA
Gold genosensor
Colorimetric assay
Non-crosslinking aggregation

ABSTRACT

Early detection of cancer increases the chance of effective treatment and survival rates. The aim of this study is to develop a rapid and non-invasive nano-biosensing method to screen common lethal cancers in their early stages. In that regard, two circulating microRNA (miR-21, miR-155) biomarkers, which are upregulated in plasma in prevalent cancers, were targeted by a rapid and colorimetric nano-biosensor based on non-crosslinking Au-nanoprobes without amplification requirement. Multiple cancerous cell lines, including A549, MCF7, HT-29, A2780, AGS, MKN-45, and SW-1736 and the primary fibroblast were examined with naked eyes after the hybridization assay using exogenous biomarkers. The results were also confirmed by spectroscopy analysis. The upregulated miRNAs in cancerous cell lines caused a significant blue shift in the Au-nanoprobe absorbance spectrum while the samples isolated from normal cells remained intact red. The limit of detection (LOD) of the method was determined to be less than one ng/μL of total isolated miRNA using an instrument-free visual method. The developed geno-sensing method could serve as a simple, point-of-care platform for cancer prognosis and diagnosis, leading to operative nano-theranostics.

1. Introduction

Due to the increasing level of cancer death each year, the main priority of many countries is spending high time and cost for diagnosis and therapy. Research shows that five-year survival increases by 10–70% only if the disease is diagnosed at early stages while still localized [1]. However, effective treatment is not possible when most cancers usually show clinical symptoms at the final fourth stage of metastasis. Therefore, early detection of cancer could increase the chance of effective therapy and recovery.

One of the important biomarkers in the blood and other body fluids is microRNA with small non-coding sequence and significant roles in alteration of post-transcriptional modification of genes. miRNAs are considered potential biomarkers because of their specific profile in many diseases, high stability in the blood and body fluids, high specificity, and being highly conserved [2]. In that regard, circulating biomarkers, including cell-free miRNAs, seem to be less invasive targets for cancer diagnosis compared with an invasive tissue biopsy, especially for cancers with inaccessible tissues for biopsy [3]. Aimed at simultaneous detection of prevalent cancers and among the miRNA dysregulations, the most common miRNA biomarkers were required. According to the latest update of the miRCancer database, the elevation of miR-21 and miR-155 were addressed in many common lethal cancers such as lung, breast, colon, pancreas, etc. [4]. Therefore, they could well serve as the general biomarkers for the detection of cancer cells. MiR-21 and miR-155 both are considered as oncomiRs. OncomiRs target the tumor suppressor genes and play essential roles in tumor cell invasiveness and resistance to apoptosis [5,6]. However, miR-155 behaves as a tumor suppressor in some other cases such as gastric and ovarian cancer [7,8].

The conventional methods for miRNA detection, including microarray, qRT-PCR, and northern blot, generally need a large amount of input miRNA and are considered to be costly, time-consuming, and sophisticated. Therefore, there is a remarkable demand for a low-cost, point-of-care method with high sensitivity and specificity [9]. Gold nanoparticles (Au-NPs) could serve as an all-in-one solution for biomarker detection due to their remarkable optical properties, various surface modifications, and biocompatibility [10,11].

Colorimetric methods of sensing oligonucleotides have attracted

* Corresponding author at: Department of Microbiology and Microbial Biotechnology, Faculty of Life Sciences and Biotechnology, Shahid Beheshti University, Velenjak, Tehran, Iran.
E-mail address: H_mollasalehi@sbu.ac.ir (H. Mollasalehi).

https://doi.org/10.1016/j.bioorg.2020.104605
Received 22 June 2020; Received in revised form 12 December 2020; Accepted 25 December 2020
Available online 31 December 2020

significant interest in molecular detection because of their simplicity, direct visualization, and rapid result [12–14]. The principle of differentiation is based on strong localized surface plasmon resonance (LSPR) characteristic of Au-NP. There are two main strategies for developing color differentiation between positive and negative samples: Crosslinking and non-crosslinking hybridization [15]. In the crosslinking Au-nanoprobes method, two nanoprobes with complementary sequences to two separate half of target DNA are employed. Hybridization of these nanoprobes with target DNA leads to the Au-NP aggregation and blue shift [16]. The non-crosslinking (NCL) method has priority over the crosslinking method because of its simplicity and quick response. Two distinct non-crosslinking aggregation mechanisms are presented: The first method was introduced by Sato and co-workers for the identification of short synthetic oligonucleotides [17]. In this method, the length of the target sequence must be of identical probe length attached to the nanoparticle. Further, in the presence of the target sequence, aggregation and blue shift occur. This phenomenon could be correlated mainly to reduced electrostatic repulsion by shielding effects of electrons resulting in increased binding affinity of the opposing ions and/ or reduction of space repulsion due to reduced entropy and harder oligonucleotide conformations. The second method was proposed by Baptista et al. for longer oligonucleotide sequences e.g. mRNA, genomic DNA, PCR products, and pathogen genes in detection approaches [18]. Unlike the first method, in the presence of the target sequence, an increase in the stability of nanoprobes and therefore, prevention of blue-shift occurs.

In this study, we developed a colorimetric nanobiosensor for simple diagnosis of prevalent lethal cancers using extracellular miRNAs. We reported the simultaneous detection of the prevalent lethal cancers using a single-tube visual assay based on non-crosslinking Au-nanoprobes. The assay was performed directly bypassing the need for a nucleic acid amplification step. In that regard, the dysregulation of two early-phase biomarkers including miR-21 and miR-155 were analyzed by two designed nanoprobes in various cancer cell lines.

2. Material and methods

2.1. Materials

Chemicals including guanidium thiocyanate, octanoic acid, 2-mercaptoethanol, and RNaseZAP were obtained from Sigma (USA). Sodium chloride (NaCl), Monosodium phosphate-monohydrate (NaH_2PO_4), Disodium phosphate- heptahydrate (Na_2HPO_4), Tris-HCl, Tris-base, Ultrapure Ethanol, $HAuCl_4$, sodium citrate, and EDTA were supplied by Merck (Germany). Tris(2-carboxyethyl) phosphine hydrochloride powder (TCEP) was purchased from BioBasic (Canada). Approximately 20–30 nm diameter spherical gold nanoparticles were provided by Fanavarane Shimi Saman, which were prepared by citrate reduction of $HAuCl_4$.The culture medium supernatant of cell lines including human lung cancer (A549), human breast adenocarcinoma (MCF7), human colon cancer (HT-29), human ovarian carcinoma (A2780 ep), human gastric cancer (AGS), human gastric cancer (MKN-45), human thyroid cancer (SW-1736) and normal human primary fibroblast cell lines was provided by the cell bank of Pasture Institute (Iran).

2.2. Synthesis and characterization of Au-NP

Gold nanoparticles were provided by Fanavarane Shimi Saman, and synthesized using thermal citrate reduction method [19] in which Au-NPs are formed by the reduction of Au salts in water using citrate ions as a reducing agent. 25 mL of the 1.0 mM $HAuCl_4$ was added to a 50 mL Erlenmeyer flask on a stirring hot plate and allowed to heat while stirring. About 2.5 mL of 38.8 mM sodium citrate was added gradually to the boiling solution. The boiling was continued for about ten minutes. As Au-NPs were formed, the solution turned deep red. In that case, the heating was stopped and stirring continued for another ten minutes.

UV–Vis spectrum of Au-NP was analyzed by Nanodrop Thermo Fisher Scientific 2000/2000c Spectrophotometer. To characterize the morphology of Au-NP, 1 mL of the synthesized Au-NP colloid was lyophilized for imaging with Hitachi SU3500 scanning electron microscope (SEM). Furthermore, the size and polydispersity index (PDI) of Au-NP were measured by Sympatech Nano Phox 90.246.V dynamic light scattering (DLS).

2.3. Designing target probes

Probe design was based on the conserved and mostly reported sequences of miR-21 and miR-155. In both biomarkers, the 5p sequence type was selected. The selected sequences were aligned using BLASTn [20] in order not to overlap with other genes. The complementary 5′-thiol modified DNA probe-1 (targeting miR-21) & probe-2 (targeting miR-155) were synthesized by Bioneer (South Korea). The final sequences of miR-21 and miR-155 and their complementary probes are mentioned in Table 1.

2.4. Au-NP functionalization

The functionalization procedure was performed to conjugate the designed probe to the surface of Au-NP [21]. In brief, to activate the thiol-modified oligonucleotides, 10 μL of 50 μM probes was mixed with 0.5 μL of 1 mM freshly prepared TCEP. The mixture was incubated for one hour at room temperature. Then 87 μL Au-NP (around 9.7 nM) was added and incubated for 16 h. Afterward, the mixture was salt-aged (gradually salt addition over one hour) in five steps with 15-minute intervals between the steps to reach the final concentration of 0.1 M NaCl and 10 mM phosphate buffer (pH = 7). Following salt addition, the mixture was incubated for 40 h at room temperature. The solution was centrifuged for 45 min in 14000 × g, and the supernatant was discarded. The precipitate was diluted in 60 μL washing buffer containing 0.1 M NaCl and 10 mM phosphate buffer (pH = 7). The last washing step was repeated three times. The DNA-functionalized Au-NPs had the same color (red) with unmodified Au-nanoprobes. However, about 25% of Au-NP would be washed away during hands-on experiments [22]. The final Au-nanoprobe concentration was determined to be around 6.5 nM. Gold nanoparticles should be stored at 4℃ until use.

2.5. miRNA isolation

Extracellular miRNAs should be isolated from other content of media such as cell debris, proteins, DNA, etc. For miRNA isolation, Gu/OcA protocol was used with some modifications. First, all cells were separated from growth media and discarded after centrifugation. 150 μL of the cell-free media was mixed with 225 μL of denaturing buffer, including 0.6 M guanidium thiocyanate and 0.5% octanoic acid. The mixture was vortexed for 5 s and incubated for 3 min at room temperature followed by centrifugation for 3 min at 10000g. Following the centrifugation step, the supernatant was mixed with an equal volume of ethanol 95%. The mixture was poured into a silica column and centrifuged for 1 min at 10000g. After the removal of flow-through, two washing steps were applied with two separate washing buffers. The first

Table 1
Sequences of microRNAs and their complementary probes.

Note	Sequence (5′→3′)
miR-21-5p	5′-UAGCUUAUCAGACUGAUGUUGA-3′
miR-155-5p	5′-UUAAUGCUAAUCGUGAUAGGGGU-3′
Probe-1 (miR-21-5p complementary)	HO—$(CH_2)_6$—S—S— $(CH_2)_6$–5′-TCAACATCAGTCTGATAAGCTA-3′
Probe-2 (miR-155-5p complementary):	HO—$(CH_2)_6$—S—S— $(CH_2)_6$–5′-ACCCCTATCACGATTAGCATTAA-3′

washing buffer included 5 M guanidium thiocyanate, 10 mM Tris-acetate (pH = 6.5), ethanol 50%, and 1% 2-mercaptoethanol. The second washing buffer contained 10 mM Tris-HCl (pH = 7.5), 0.1 mM NaCl, and 75% ethanol. After centrifugation, the flow-through was discarded. To elute the miRNA from the silica column, 120 μL of TE buffer (10 mM Tris-HCl, 1 mM EDTA, pH = 8) was added and centrifuged for 15 min at 4000g. The final flow-through contained isolated miRNAs.

DEPC-treated (0.1%) deionized water was used in all experiments. All plastics and glass vessels were cleaned by RNaseZAP to complete the removal of RNase contamination.

2.6. Colorimetric detection of target miRNA

Prior to the detection assay, the concentration of isolated RNA was measured by Nanodrop and normalized to 4 ng/ μL. 0.5 μL of isolated miRNA (4 ng/μL) was added to 4 μL of Au-nanoprobes, including Au-nanoprobe-1 and 2 in separate microtubes. The solution was incubated at 65C for 2 min, followed by 3 min incubation at 50C. After hybridization, 0.5 μL NaCl 4 M was added to the tube. Samples related to cancer and normal cell lines were handled separately under all identical experimental conditions. The negative control sample contained human normal fibroblast, and the blank sample contained TE buffer without nucleic acid. The color change was detectable significantly without any sophisticated instruments two seconds after salt induction. However, the sample solutions were investigated by spectrophotometer for quantitative analysis. We scanned and analyzed the SPR band of a positive (aggregated) and negative (non-aggregated) Au-nanoprobes and designated the aggregation peak of 650 nm and non-aggregation peak of 520 nm as the most appropriate wavelength for further investigation. Finally, the aggregation absorption wavelength of 650 nm was selected for the end-point analysis and point-to-point comparison (Supplementary Fig. 1).

2.7. Reliability analysis

For assessment of exact sequences of miRNAs and the corresponding probes, miR-21 and miR-155 reverse complementary sequences were synthesized and used as specific target of Au-nanoprobes in the colorimetric assay. To maintain consistency of the results, we diluted the synthesized oligonucleotides to the mean concentration of isolated miRNA from samples (4 ng/μL). The colorimetric assay was performed identically to the real samples and final results were transferred onto a Whatman filter paper for a better resolution.

2.8. Determination of detection limit

To investigate the minimum required amount of miRNA for the visible color change, a serial dilution of the isolated RNA from breast cancer cell line in TE buffer was prepared in five microtubes. The concentration of the extracted miRNAs was 20 ng/ μL. However, it was normalized to working concentration of 4 ng/ μL. Finally, the diluted concentrations of 2, 1.5, 1, and 0.8 ng/ μL were prepared and a fixed appropriate volume was added to Au-nanoprobe 1. After salt induction, the colorimetric differentiation of the series was analyzed.

2.9. Statistical analysis

The provided experimental test were performed in at least triplicates under identical experimental condition and the expressed data were the mean ± standard error of the mean. Statistical analysis was performed using *t*-test to determine significant differences between the means of sample groups. Values with $P \leq 0.05$ were considered statistically significant and accepted.

3. Results

Gold nanoparticles were conjugated to the complementary oligonucleotides to target the extracellular miRNA biomarkers for the direct diagnosis of common lethal cancers. Color differentiation is based on the salt-induced blue shift of Au-nanoprobes upon complementary hybridization, which is correspondent to upregulation of target miRNAs. All colorimetric assays were performed on normalized concentrations of isolated RNAs.

3.1. Au-NP characterization and conjugation

The presence and dispersion of Au-NP before and after functionalization was recorded by UV–Vis spectroscopy scanning 300–800 nm. It illustrated the maximum peak of 520 nm which was related to the monodisperse (not aggregated) state of particles and nanoprobes (Fig. 1a). The spherical morphology and required size of Au-NP was determined and confirmed before and after conjugation with oligonucleotide probes by transmission electron microscopy (TEM) (Fig. 1b). It was revealed that after functionalization with probes, the particles seemed to be more disperse than Au-NP because of increased charge density around Au. The mean size of Au-NP was measured to be 23.30 nm, and also the polydispersity index (PDI) of particles was calculated to be 0.02, which indicated limited particle size distribution (Fig. 1c).

For stability analysis and to confirm the conjugation of oligonucleotides to Au-NP, the salt induction assay was performed for both bare Au-NP and Au-nanoprobes. The test is based on the increased anionic density around Au-nanoprobes in comparison to AuNP subsequent to successful functionalization. The bare Au-NP aggregated in concentration of 0.02 M NaCl and the solution turned blue. However, at that concentration, Au-nanoprobes did not change in color and absorption wavelength (with maximum absorbance peak at 524 nm) up to the concentration of 0.1 M NaCl.

3.2. Colorimetric assay

In the colorimetric assay, three samples (test, negative, and control) were prepared. The isolated miRNA of each cell line with normalized concentration was added to separate microtubes, including Au-nanoprobe 1 or Au-nanoprobe 2. After hybridization procedure and salt adjustment, all cancerous samples in the case of Au-nanoprobe-1 appeared as blue/gray. In a parallel approach with Au-nanoprobe-2, the samples related to A549, MCF7, HT29, and SW1736 appeared as blue/gray, the sample related to A2780ep appeared as purple-blue and MKN-45 was observed as red- purple, while AGS sample displayed red (Fig. 2). All experiments were carried out using at least three samples. The UV–visible absorbance of all samples was recorded at 650 nm for further quantitative comparative analysis (Fig. 2). Both negative samples comprising normal cell line of human primary fibroblast and control blank samples did not display any color alteration. The complete results of these two nanoprobes were shown in Table 2.

It should be noted that both blue and purple were considered positive results because of the blue shift in UV–Vis wavelength absorption (Fig. 2).

3.3. Sensitivity and reliability of the colorimetric assay

This assay was conducted on the serially diluted amount of normalized isolated RNA to determine the LOD of the assay. The least concentration of target miRNA that could induce visual color change and differentiation detectable by naked eyes was considered LOD of the assay. The color change was detectable significantly at or above one ng/ μL diluted RNA, as shown in Fig. 3. There is a time dependency on the quality and intensity of color change in Au-nanoprobes. In that regard, as the time increases after salt induction, some portions of aggregates tend to precipitate (in black). Although the differentiation of color

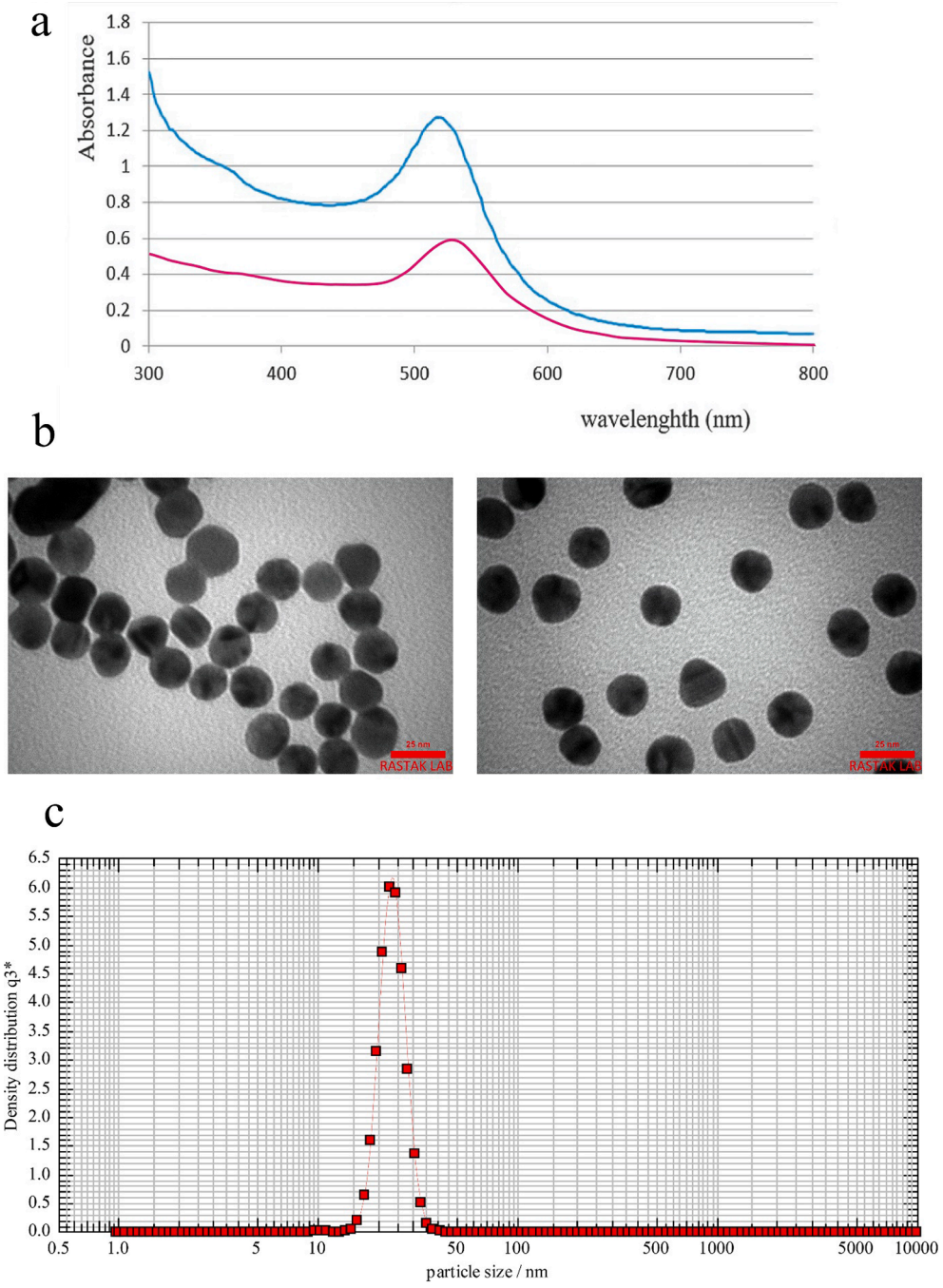

Fig. 1. Characterization of Au-NP and Au-nanoprobes. (a) UV –Vis spectrum of bare Au-NP (blue/top) and Au-nanoprobe (red/bottom), the maximum absorption is 520 nm; (b) Transmission electron microscope (TEM) images of Au-NP (left) vs. Au-nanoprobes (right) at the scale of 25 nm; (c) Dynamic light scattering (DLS) analysis of size distribution of the prepared Au-NP. (For interpretation of the references to color in this figure legend, the reader is referred to the web version of this article.)

between samples was started and detectable after two seconds, however, qualitative analysis of the samples was recorded after some intervals to reach the best visual differentiation e.g., ten minutes after salt induction. It should be noted that the minimum reported amount of miRNA corresponds to total miRNA in which the target miRNA is a portion. In that regard, it could be claimed that the detection limit of the developed method is less than one ng/μL. All experiments were carried out using at least three identical repeats.

For assessment of the reliability of the colorimetric assay, synthesized sequences of miR-21 and miR-155 (reverse complementary sequences of each nanoprobe) were hybridized to Au-nanoprobes. The results on Whatman filter paper showed that Au-nanoprobe 1 and 2 could significantly induce color change to purple/gray upon hybridization to their target complementary sequences (Fig. 4).

4. Discussion

In this study, extracellular dysregulated miRNAs were detected colorimetrically using the non-crosslinking method of Au-nanoprobes. Since the target molecules were 19–24 bp length, the identical hybridization non-crosslinking assay was expected for the aggregation mechanism. In 2010, this method was used for detection of chronic myeloid leukemia (CML) with targeting fusion BCR-ABL mRNA [23] and the sensitivity was reported as 10 ng/μL of total human RNA. However, to the best of our knowledge, this is the first report on the usage of the NCL aggregation method for the simultaneous detection of common cancers by targeting unamplified miRNA molecules. The conjugation of target miRNAs to their complementary Au-nanoprobes results in their aggregation and blue shift which could be visualized by naked eyes and recorded by spectrophotometric comparison of color before and after

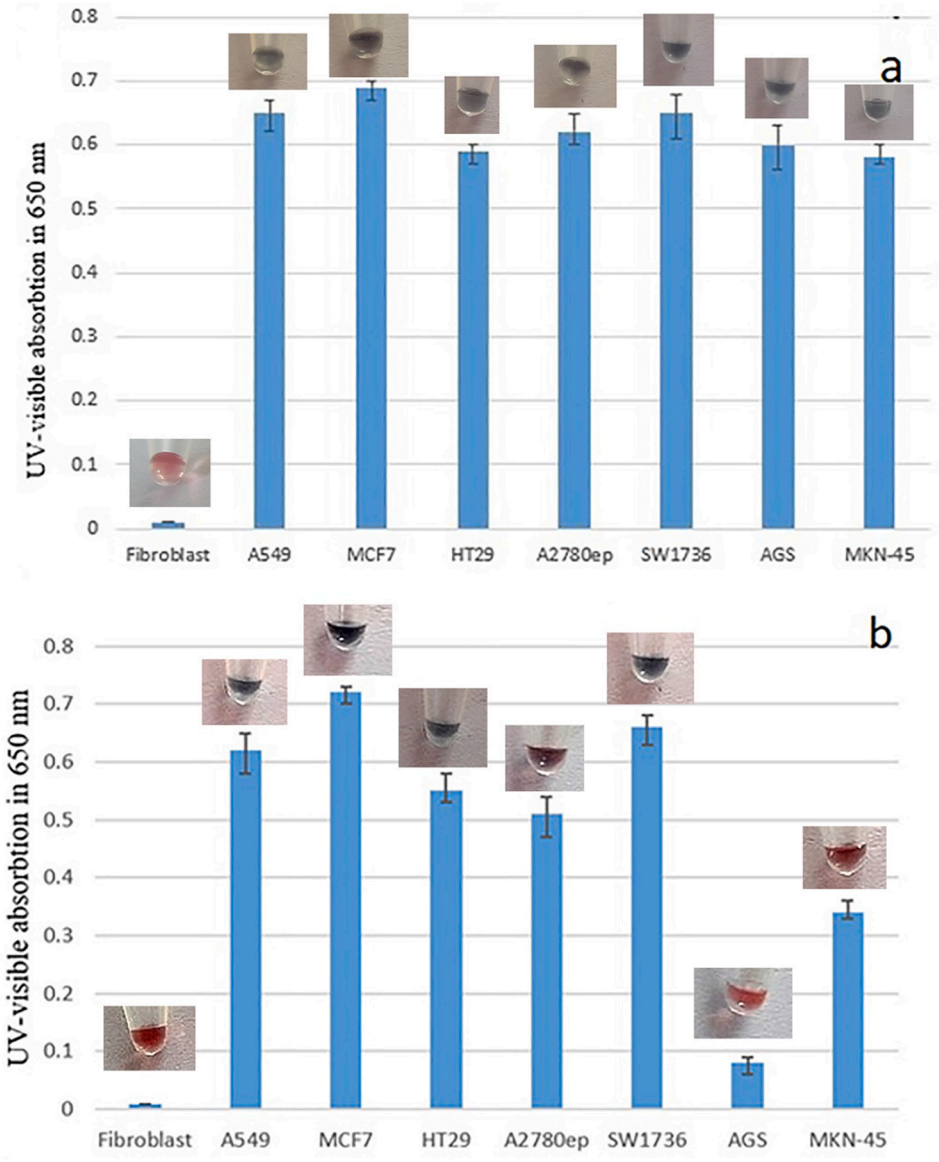

Fig. 2. The recorded UV–visible absorbance at 650 nm and the corresponding colorimetric differentiation of the isolated miRNA samples using Au-nanoprobe-1 and 2. a) Au-nanoprobe-1b) Au-nanoprobe-2. The sample related to normal fibroblast cell lines shows almost no absorbance at 650 nm. However, other cancerous cell lines show a detectable blue shift. Samples comprised normal human fibroblast, human lung cancer (A549), human breast adenocarcinoma (MCF7), colon cancer (HT29), human ovarian carcinoma (A2780ep), human thyroid cancer (SW1736), human gastric cancer (AGS), human gastric cancer (MKN-45). (For interpretation of the references to color in this figure legend, the reader is referred to the web version of this article.)

Table 2
The color of nanoprobes after hybridization assay in different cell lines.

Cancer	Cell line	Nanoprobe-1	Nanoprobe-2
Control	_	Red	Red
Normal	Primary fibroblast	Red	Red
Lung	A549	Blue	Blue
Breast	MCF7	Blue	Blue
Colon	HT29	Blue	Blue
Ovarian	A2780ep	Blue	Purple- Blue
Thyroid	SW1736	Blue	Blue
Gastric	AGS	Blue	Red
Gastric	MKN-45	Blue	Red- Purple

salt induction procedure. This is a user-friendly method without the need for any miRNA amplification and sophisticated instruments and takes less than ten minutes to get the results after RNA isolation. The whole detection process minimizes the RNA downstream hands-on and possible RNA degradation. Furthermore, low volumes of primary sample are needed, which could be a valuable advantage in future studies of non-invasive sampling of cancerous patients. We used the culture media of cell lines to collect their extracellular miRNAs rather than using synthetic miRNAs to reach more reliable results. Given that extracellular miRNAs are accompanied by proteins and/or lipoproteins, in this study we designed an effective isolation method to access miRNAs in appropriate concentrations. Colorimetric assay with nanoprobe-1 (miR-21) revealed all cancerous samples to be distinguishable obviously from primary fibroblast cells within one minute of salt addition.

According to the previous quantitative RT-PCR gene expression analysis of the target miR-21 and miR-155 in the selected cell lines, the higher expression of miR-21 in A549 (lung cancer) cell line in comparison to the normal human bronchial epithelial cells was reported [24]. Meng et al. analyzed the expression of miR-21 in colorectal cancer cell lines including HT-29 and evaluated the effects of anti-miR-21 on cell proliferation, migration, and invasion [25]. Similarly, many other studies measured the quantitative expression of miR-21 in MCF-7 breast cancer cell lines [26,27], SW1736 thyroid cancer cell lines [28], AGS, and MKN-45 gastric cancer cell lines [29]. There are similar data for quantitively measuring of miR-155 which indicate the higher expression in various cancer cell lines such as A549 [30], MCF-7 [31], HT-20 [32]. Moreover, the upregulation of miR-21 was reported in all common cancers, including breast [33], colon [34], ovary [35], lung [36] and gastric [37]. On the other hand, the assay of nanoprobe-2 (miR-155)

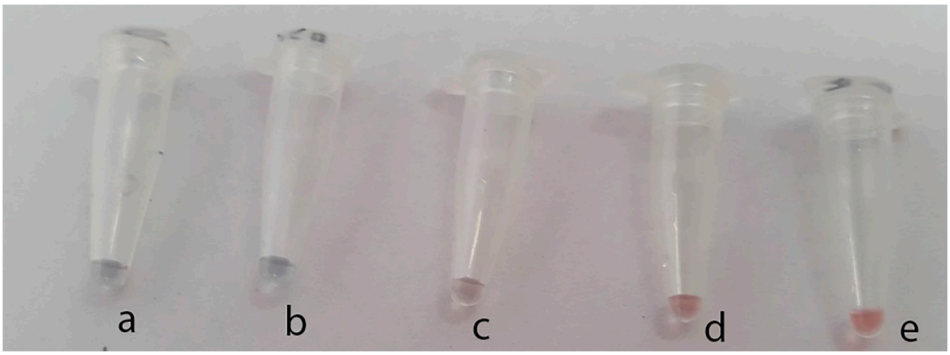

Fig. 3. Serially diluted RNA samples to discriminate the minimum detectable concentration by unequipped eyes. a: 4 ng/μL, b: 2 ng/μL, c: 1.5 ng/μL, d: 1 ng/μL, e: 0.8 ng/μL. The color change was obviously detectable within ten minutes after salt addition at or above one ng/μL.

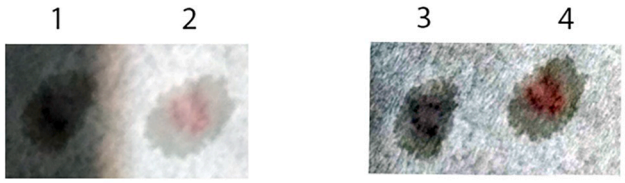

Fig. 4. Reliability test. Reliability test was performed using miR-21 and miR-155 sequences and the colorimetric assay. It was shown that color change from red to purple/gray occurs upon salt addition following hybridization. Pattern 1 corresponds to Au-nanoprobe 1, pattern 2, blank sample, pattern 3 is Au-nanoprobe 2 and pattern 4, blank sample. (For interpretation of the references to color in this figure legend, the reader is referred to the web version of this article.)

showed a different pattern of color alteration. Lung, breast, colon, and thyroid samples changed to the blue, ovary and gastric sample (MKN-45) were purple, and AGS (gastric) displayed red. This observation could be correlated to the different concentrations of miR-155 in the samples. Upregulation of miR-155 in most cancers such as lung [36], breast [38], colon [39], and thyroid [40] has been reported. Hou and co-workers introduced miR-155 as a cancer diagnostic biomarker with the highest accuracy in breast cancer compared to other types of cancers [5]. This is in accordance with our findings for the MCF-7 sample with extensive aggregation. However, in the case of gastric cancer, some studies indicated the upregulation of miR-155 in AGS and MKN-45 cell lines [41,42], and other studies demonstrated the downregulation of this biomarker [8,43]. The color alteration in the sample of MKN-45 was very slight, which shows small upregulation of miR-155. No color alteration was detected in AGS sample, which indicated the downregulation of miR-155. In addition, some other studies have reported the downregulation of miR-155 in ovarian cancer [7,44,45] while it was found to be increased (blue shift) in this study. Therefore, according to previous studies and our results, it could be claimed that evaluating miR-155 separately in gastric and ovarian cancers could not serve as a proper diagnostic biomarker. This indicates that targeting miR-21 biomarker could be sufficient for detecting cancer and detecting miR-155 along with miR-21 could help increase the accuracy of the test.

5. Conclusions

In this study, we presented a rapid and sensitive method for the detection of extracellular miRNAs based on colorimetric non-crosslinking hybridization of gold nanoprobes. The results revealed a nanogram per microliter scale of sensitivity for total miRNA isolated from the cultured cells in media without the necessity of miRNA reverse transcription, labeling, and amplification. Besides, the distinction of the dysregulation of miRNAs could be assessed with naked eyes. Therefore, the presented platform is an easy-to-perform technique without the need for sophisticated equipment that could be applied to cancer detection with high sensitivity and specificity. This technique could also serve as an appropriate universal mean of cancer screening tests to help patients receive early and effective therapy.

Author contributions

HM designed the experiment, interpreted the results and helped write the manuscript. ESH performed the experiment, analyzed the data and wrote the first draft of the manuscript.

Declaration of Competing Interest

The authors declare that they have no known competing financial interests or personal relationships that could have appeared to influence the work reported in this paper.

Acknowledgments

This work was financially supported by cancer control research center, cancer control foundation, Iran university of medical sciences, Tehran, Iran, as project No: CCF-97092. The authors also appreciate supports of Shahid Beheshti University.

Data availability

The authors confirm that the data supporting the findings of this study are available within the article [and/or] its supplementary materials.

Appendix A. Supplementary material

Supplementary data to this article can be found online at https://doi.org/10.1016/j.bioorg.2020.104605.

References

[1] R. Alteri, T. Bertaut, D. Brooks, W. Chambers, E. Chang, M. Chen, Cancer Facts and Figures is an annual publication of the American Cancer Society, Atlanta, Georgia. (Table 8) (2016) 23.
[2] N. Kosaka, H. Iguchi, T. Ochiya, Circulating microRNA in body fluid: a new potential biomarker for cancer diagnosis and prognosis, Cancer Sci. 101 (10) (2010) 2087–2092.
[3] H.M. Heneghan, N. Miller, A.J. Lowery, K.J. Sweeney, J. Newell, M.J. Kerin, Circulating microRNAs as novel minimally invasive biomarkers for breast cancer, Ann. Surg. 251 (3) (2010) 499–505.
[4] E. Shajari, H. Mollasalehi, Ribonucleic-acid-biomarker candidates for early-phase group detection of common cancers, Genomics 112 (1) (2020) 163–168.
[5] Y. Hou, J. Wang, X. Wang, S. Shi, W. Wang, Z. Chen, Appraising microRNA-155 as a noninvasive diagnostic biomarker for cancer detection: a meta-analysis, Medicine 95 (2) (2016).

[6] Y. Wang, X. Gao, F. Wei, X. Zhang, J. Yu, H. Zhao, Q. Sun, F. Yan, C. Yan, H. Li, Diagnostic and prognostic value of circulating miR-21 for cancer: a systematic review and meta-analysis, Gene 533 (1) (2014) 389–397.
[7] W. Chen, L. Huang, C. Hao, W. Zeng, X. Luo, X. Li, L. Zhou, S. Jiang, Z. Chen, Y. He, MicroRNA-155 promotes apoptosis in SKOV3, A2780, and primary cultured ovarian cancer cells, Tumor Biol. 37 (7) (2016) 9289–9299.
[8] H. Li, S. Xie, M. Liu, Z. Chen, X. Liu, L. Wang, D. Li, Y. Zhou, The clinical significance of downregulation of mir-124-3p, mir-146a-5p, mir-155-5p and mir-335-5p in gastric cancer tumorigenesis, Int. J. Oncol. 45 (1) (2014) 197–208.
[9] A. Mitchell, A.M. James, T. Alexy, G. Bao, C.D. Searles, Detection and Assessment of MicroRNA Expression in Human Disease, in: RNA and DNA Diagnostics, Springer, 2015, pp. 333–349.
[10] W. Lee, S.M. Shaban, D.G. Pyun, D.-H. Kim, Solid-phase colorimetric aptasensor for thrombin detection, Thin Solid Films 686 (2019), 137428.
[11] D.J. de Aberasturi, A.B. Serrano-Montes, L.M. Liz-Marzán, Modern applications of plasmonic nanoparticles: from energy to health, Adv. Opt. Mater. 3 (5) (2015) 602–617.
[12] S.M. Shaban, J.Y. Lee, D.-H. Kim, Dual-Surfactant-Capped Ag Nanoparticles as a Highly Selective and Sensitive Colorimetric Sensor for Citrate Detection, ACS Omega (2020).
[13] Y. Song, W. Wei, X. Qu, Colorimetric biosensing using smart materials, Adv. Mater. 23 (37) (2011) 4215–4236.
[14] D. Vilela, M.C. González, A. Escarpa, Sensing colorimetric approaches based on gold and silver nanoparticles aggregation: chemical creativity behind the assay. A review, Analytica chimica acta 751 (2012) 24–43.
[15] R. Elghanian, J.J. Storhoff, R.C. Mucic, R.L. Letsinger, C.A. Mirkin, Selective colorimetric detection of polynucleotides based on the distance-dependent optical properties of gold nanoparticles, Science 277 (5329) (1997) 1078–1081.
[16] W. Zhao, M.A. Brook, Y. Li, Design of gold nanoparticle-based colorimetric biosensing assays, ChemBioChem 9 (15) (2008) 2363–2371.
[17] K. Sato, K. Hosokawa, M. Maeda, Rapid aggregation of gold nanoparticles induced by non-cross-linking DNA hybridization, J. Am. Chem. Soc. 125 (27) (2003) 8102–8103.
[18] P. Baptista, G. Doria, D. Henriques, E. Pereira, R. Franco, Colorimetric detection of eukaryotic gene expression with DNA-derivatized gold nanoparticles, J. Biotechnol. 119 (2) (2005) 111–117.
[19] J. Turkevich, P.C. Stevenson, J. Hillier, A study of the nucleation and growth processes in the synthesis of colloidal gold, Discuss. Faraday Soc. Special 11 (1951) 55–75.
[20] U.S.N.L.o. Medicine, Nocleotide BLAST, National Center for Biotechnology Information (NCBI), Basic local alignment search tool, 2019 10 Dec. https://blast.ncbi.nlm.nih.gov/Blast.cgi?PAGE_TYPE=BlastSearch.
[21] T.A. Taton, Preparation of gold nanoparticle–DNA conjugates, Current Protocols Nucleic Acid Chem. 12 (2) (2002), pp. 1–12.2. 12.
[22] J.J. Storhoff, R. Elghanian, R.C. Mucic, C.A. Mirkin, R.L. Letsinger, One-pot colorimetric differentiation of polynucleotides with single base imperfections using gold nanoparticle probes, J. Am. Chem. Soc. 120 (9) (1998) 1959–1964.
[23] J. Conde, J.M. de la Fuente, P.V. Baptista, RNA quantification using gold nanoprobes-application to cancer diagnostics, J. Nanobiotechnol. 8 (1) (2010) 5.
[24] Q. Sun, M. Hang, X. Guo, W. Shao, G. Zeng, Expression and significance of miRNA-21 and BTG2 in lung cancer, Tumor Biol. 34 (6) (2013) 4017–4026.
[25] C. Li, L. Zhao, Y. Chen, T. He, X. Chen, J. Mao, C. Li, J. Lyu, Q.H. Meng, MicroRNA-21 promotes proliferation, migration, and invasion of colorectal cancer, and tumor growth associated with down-regulation of sec23a expression, BMC cancer 16 (1) (2016) 1–11.
[26] L.X. Yan, Q.N. Wu, Y. Zhang, Y.Y. Li, D.Z. Liao, J.H. Hou, J. Fu, M.S. Zeng, J.P. Yun, Q.L. Wu, Knockdown of miR-21 in human breast cancer cell lines inhibits proliferation, in vitro migration and in vivotumor growth, Breast Cancer Res. 13 (1) (2011) R2.
[27] S. Zhu, H. Wu, F. Wu, D. Nie, S. Sheng, Y.-Y. Mo, MicroRNA-21 targets tumor suppressor genes in invasion and metastasis, Cell Res. 18 (3) (2008) 350–359.
[28] V. Haghpanah, P. Fallah, R. Tavakoli, M. Naderi, H. Samimi, M. Soleimani, B. Larijani, Antisense-miR-21 enhances differentiation/apoptosis and reduces cancer stemness state on anaplastic thyroid cancer, Tumor Biol. 37 (1) (2016) 1299–1308.
[29] M. Bakhshi, J. Asadi, M. Ebrahimi, A.V. Moradi, M. Hajimoradi, Increased expression of miR-146a, miR-10b, and miR-21 in cancer stem-like gastro-spheres, J. Cell. Biochem. 120 (10) (2019) 16589–16599.
[30] S. Gu, Y. Lai, H. Chen, Y. Liu, Z. Zhang, miR-155 mediates arsenic trioxide resistance by activating Nrf2 and suppressing apoptosis in lung cancer cells, Sci. Rep. 7 (1) (2017) 1–13.
[31] C.-M. Zhang, J. Zhao, H.-Y. Deng, MiR-155 promotes proliferation of human breast cancer MCF-7 cells through targeting tumor protein 53-induced nuclear protein 1, J. Biomed. Sci. 20 (1) (2013) 79.
[32] A.A. Al-Haidari, I. Syk, H. Thorlacius, MiR-155-5p positively regulates CCL17-induced colon cancer cell migration by targeting RhoA, Oncotarget 8 (9) (2017) 14887.
[33] F.M. Badr, Potential role of miR-21 in breast cancer diagnosis and therapy, Biotechnol. Bioeng. 3 (5) (2016) 1068–1075.
[34] Y. Wu, Y. Song, Y. Xiong, X. Wang, K. Xu, B. Han, Y. Bai, L. Li, Y. Zhang, L. Zhou, MicroRNA-21 (Mir-21) promotes cell growth and invasion by repressing tumor suppressor PTEN in colorectal cancer, Cell. Physiol. Biochem. 43 (3) (2017) 945–958.
[35] C. Palma Flores, R. García-Vázquez, D. Gallardo Rincón, E. Ruiz-García, H. Astudillo de la Vega, L.A. Marchat, Y.M. Salinas Vera, C. López-Camarillo, MicroRNAs driving invasion and metastasis in ovarian cancer: Opportunities for translational medicine, Int. J. Oncol. 50 (5) (2017) 1461–1476.
[36] X. Xue, Y. Liu, Y. Wang, M. Meng, K. Wang, X. Zang, S. Zhao, X. Sun, L. Cui, L.J. O. Pan, MiR-21 and MiR-155 promote non-small cell lung cancer progression by downregulating SOCS1, SOCS6, and PTEN, Oncotarget 7 (51) (2016) 84508.
[37] B.G. Zhang, J.F. Li, B.Q. Yu, Z.G. Zhu, B.Y. Liu, M. Yan, MicroRNA-21 promotes tumor proliferation and invasion in gastric cancer by targeting PTEN, Oncol. Rep. 27 (4) (2012) 1019–1026.
[38] S. Mattiske, R.J. Suetani, P.M. Neilsen, D.F. Callen, P. Biomarkers, The oncogenic role of miR-155 in breast cancer, Cancer Epidemiol. Biomarkers Prev. 21 (8) (2012) 1236–1243.
[39] H. Cao, S. Huang, A. Liu, Z. Chen, Up-regulated expression of miR-155 in human colonic cancer, J. Cancer Res. Ther. 14 (3) (2018) 604.
[40] X. Zhang, M. Li, K. Zuo, D. Li, M. Ye, L. Ding, H. Cai, D. Fu, Y. Fan, Lv. Zhongwei, Upregulated miR-155 in papillary thyroid carcinoma promotes tumor growth by targeting APC and activating Wnt/β-catenin signaling, J. Clin. Endocrinol. Metab. 98 (8) (2013) E1305–E1313.
[41] H. Wei, Y. Li, Q. Ning, Z.M. Suo, Regulation of miR-155 affects the invasion and migration of gastric carcinoma cells by modulating the STAT3 signaling pathway, Oncol. Lett. 16 (4) (2018) 4137–4142.
[42] Y. Qu, H. Zhang, W. Sun, Y. Han, S. Li, Y. Qu, G. Ying, Y. Ba, Micro RNA-155 promotes gastric cancer growth and invasion by negatively regulating transforming growth factor-β receptor 2, Cancer Sci. 109 (3) (2018) 618–628.
[43] C.L. Li, H. Nie, M. Wang, L.P. Su, J.F. Li, Y.Y. Yu, M. Yan, Q.L. Qu, Z.G. Zhu, B. Y. Liu, microRNA-155 is downregulated in gastric cancer cells and involved in cell metastasis, Oncol. Rep. 27 (6) (2012) 1960–1966.
[44] W. Qin, Q. Ren, T. Liu, Y. Huang, J.J.F.l. Wang, MicroRNA-155 is a novel suppressor of ovarian cancer-initiating cells that targets CLDN1, FEBS Lett. 587 (9) (2013) 1434–1439.
[45] K.E. Resnick, H. Alder, J.P. Hagan, D.L. Richardson, C.M. Croce, D.E. Cohn, The detection of differentially expressed microRNAs from the serum of ovarian cancer patients using a novel real-time PCR platform, Gynecol. Oncol. 112 (1) (2009) 55–59.